Zhang *et al. Immunity & Ageing* (2025) 22:18
https://doi.org/10.1186/s12979-025-00513-z

Immunity & Ageing

RESEARCH Open Access

The immunological age prediction of monocytes indicates that gestational diabetes mellitus accelerates the aging of monocytes in offspring

Yan Zhang[1], Rui Guo[1], Min Yin[1,2], Mei Shi[1], Ting Zhong[1], Shanshan Liu[1] and Xia Li[1*†]

Abstract

Background Recent studies have suggested that gestational diabetes mellitus (GDM) can accelerate cellular aging in multiple cell types in offspring, but its impact on immune senescence remains uncertain. Our prior study reveals GDM increased the secretion of inflammatory factors by monocytes in offspring. This study discovered the transcriptome characteristics of aging monocytes at the single-cell level and explore the impact of GDM on the progression of monocyte aging in offspring.

Method Single-cell sequencing data from 56 healthy individuals (aged 0-100 years), comprising self-measured samples ($n=6$) and publicly available datasets from the Gene Expression Omnibus (GEO, $n=50$), were analyzed to characterize monocyte senescence. Linear mixed-effects modeling was used to screen for age-related genes. A random forest model was created to predict immune age in monocytes, allowing for quantitative assessment of aging.

Results We detected an increase in the number of inflammatory monocytes expressing IL1B and CXCL8 with age. Two age-related gene expression patterns were identified in monocytes. Analysis of offspring monocytes from mothers with GDM suggested that exposure to a GDM environment in the womb may lead to increased expression of aging-related genes, a hindered cell cycle, and increased immune age. The immune age of monocytes at birth is significantly linked to maternal weight gain, high fasting blood glucose levels, and cord blood C-peptide levels during pregnancy.

Conclusions Exposure to GDM during pregnancy accelerates aging in offspring immune cells. Monitoring maternal weight and blood sugar during GDM can help prevent negative effects on the offspring immune system.

Keywords Gestational diabetes, Umbilical cord blood, Immune senescence, Monocytes

†Xia Li should consider as Lead contact.

*Correspondence:
Xia Li
lixia@csu.edu.cn
[1]National Clinical Research Center for Metabolic Diseases, Key Laboratory of Diabetes Immunology, Ministry of Education, and Department of Metabolism and Endocrinology, The Second Xiangya Hospital of Central South University, Changsha, China
[2]Department of Nutritional, The Second Xiangya Hospital of Central South University, 139 Renmin Zhong Road, Changsha 410011, Hunan, China

Introduction

Gestational diabetes mellitus (GDM) is a common metabolic disorder during pregnancy that increases the likelihood of enduring health implications in offspring [1], such as diabetes, obesity, and cardiovascular diseases [2–8]. Recent research has indicated that GDM can expedite cellular aging in various types of cells in offspring, including muscle cells, endothelial cells, and mesenchymal stem cells [9–11]. Nevertheless, there is a dearth of studies exploring the potential influence of GDM on immunosenescence in offspring. Previous research has indicated elevated levels of inflammatory markers in the umbilical cord serum of GDM offspring, as well as shortened telomeres in leukocytes [12].

Cellular senescence involves cell cycle arrest [13], changes in cell morphology and metabolism, shortened telomeres, and chromatin remodeling [14]. These changes affect immune cell composition and function, leading to increased expression of senescence markers and a senescence-associated secretory phenotype (SASP) [15]. Our prior investigation utilizing single-cell sequencing techniques substantiated the influence of GDM on the increased secretion of inflammatory factors by monocytes in offspring, resulting in alterations in the monocyte inflammatory phenotype and immune function [16]. Monocytes play a key role in the immune response and inflammation [17], with changes in their proportions in elderly individuals linked to increased rates of chronic inflammation and age-related diseases such as atherosclerosis [18–21]. We hypothesized that the heightened inflammation observed in monocytes of offspring born to mothers with GDM may be attributed to the induction of immunosenescence by the GDM environment, potentially resulting in adverse long-term consequences. However, it is not clear whether GDM can accelerate monocyte senescence in offspring.

Although the characteristics of aging lymphocytes are known [22], those of aging monocytes are still unclear. Machine learning techniques are used to estimate cell age and develop predictive models of immune cell aging based on environmental factors [23–27]. In recent studies, there has been a growing trend in utilizing single-cell sequencing data and multiomics data to construct predictive models of immune cell aging [28, 29]. Nevertheless, the current predictive training samples for immune age prediction are primarily from adults and may not accurately predict immune cell age in children or infants. Therefore, there is a need for more precise predictive models to assess the effects of the GDM environment on offspring immune age.

This study will discover single-cell transcriptome characteristics of monocytes from various age cohorts and establish a predictive model of monocyte immune age. Furthermore, we will explore the impact of maternal exposure to GDM environments during fetal development on the aging process of umbilical cord monocytes.

Materials and methods

Study population

The study cohort comprised 3 healthy mothers and 4 patients with GDM from whom cord blood samples were obtained between October and December 2020 at the Second Xiangya Hospital of Central South University. Additionally, peripheral blood samples were collected from 3 healthy children aged 0–10 years for single-cell sequencing analysis. The corresponding sample information has been reported previously [16, 30]. Other samples were sourced from four publicly accessible datasets in the Gene Expression Omnibus (GEO) database: (1) GSE158055 [31] containing single-cell sequencing data of PBMCs from 20 healthy controls; (2) GSE157007 [32] containing single-cell sequencing data of PBMCs from 9 healthy adults; (3) GSE135779 [33] containing single-cell sequencing data of PBMCs from 16 healthy subjects; and (4) GSE206283 [34] containing single-cell sequencing data of PBMCs from healthy controls and COVID-19 patients upon their first hospital admission.

Definition of individuals without health conditions: For the healthy controls recruited: Participants were systematically enrolled through advertisements placed at certified preschool education institutions and tertiary medical centers. Each volunteer underwent comprehensive medical history evaluation with specific exclusion of: (1) diabetes mellitus, (2) active infections, (3) autoimmune disorders, (4) hepatic or renal dysfunction, and (5) steroid hormone use within 3 months. Database-derived subjects: Health status was verified by referencing original publications.

The research conducted in this study received approval from the Research Ethics Committee of the Second Xiangya Hospital of Central South University (Approval No. SQ2016YFSF110035) and adhered to the principles outlined in the Helsinki Declaration. Prior to participation, all individuals involved in the experiment provided written informed consent. Details of the self-test data used in this research were provided in a previous study [16]. Supplementary Table 1 provides basic information for all datasets within this chapter, and Supplementary Table 2 lists the age and gender of all participants.

Data processing and quality control for single-cell RNA sequencing

The gene barcode matrix from all the samples was combined using the R package Seurat V3. Sequencing information for each sample can be found in our previous reports [16]. For quality control, we rigorously selected high-quality cells based on the following criteria: (1) a minimum threshold of 200 and maximum threshold of

4,500 unique genes detected per cell (nFeature_RNA); (2) mitochondrial gene content not exceeding 15% of total counts.

Dimension reduction and major cell type annotation

Highly variable genes were identified using the FindVariableFeatures function (default parameters). The RunPCA function in Seurat V3 was used to perform principal component analysis (PCA) on the top 2000 variable genes. Batch effects were removed using the R package Harmony version 1.0 based on the top 50 PCA components identified. The first 50 principal components were then used for cell clustering and uniform manifold approximation and projection (UMAP) [35] dimensional reduction. Cluster marker genes were recognized using the FindAllMarkers function, and clusters were manually annotated using known cell-type marker genes [36]. The cell cycle status of each cell was predicted using the CellCycleScoring function, and the cell cycle gene set used was the cc.genes.updated.2019 gene set in Seurat.

Monocytes, granulocytes, T cells, B cells, and other immune cells were identified from mononuclear cells for further subclustering. Following isolation, PCA and clustering were performed in the manner described in the dimension reduction and major cell type annotation section.

Detection of differentially expressed genes and functional enrichment analysis

Differential gene expression (DEG) analysis was carried out in Seurat using the FindMarkers function with the Wilcoxon test, and *p* values were adjusted by using Bonferroni correction. DEGs were ranked by average log2 (fold change) after filtering with a minimum|log2(fold change)| of 0.585 and a maximum adjusted *p* value of 0.05. GSEA was performed using OmicStudio tools, which can be found at https://www.omicstudio.cn/. Pear son correlation was utilized to assess the similarity of cell groups to identify similar functional clusters.

AUCell analysis

To determine whether the activation of certain pathways differs between cells, the AUCell R package [37] was utilized to calculate the degree of pathway activation for each cell using gene set enrichment analysis. The area under the curve (AUC) of gene expression in the selected pathway was calculated using a specific gene list downloaded from the GSEA database [38]. Cells that expressed more genes within the gene set had relatively high AUC values. Therefore, gene expression rankings for each cell were generated based on the AUC. The "AUCell_exploreThresholds" function was utilized to determine the threshold for identifying gene set active cells. To visualize the active clusters, the AUC of each cell was mapped to the UMAP embedding using the ggplot2 R package (version 3.3.5) [39].

Cytotrace

To predict the relative differentiation state of cells, we performed CytoTRACE (v0.1.0) analysis [40] based on the monocyte subclustering data.

Functional enrichment analysis

GO enrichment analysis was performed using DAVID bioinformatics tools, which can be found at https://david.ncifcrf.gov/.

Linear fitting

To acquire continuous change curves depicting the predicted age for individual monocyte clusters and assess the predictive efficiency in relation to the number of variables, linear fitting graphs were created utilizing the heatmap function on the web-based data analysis and visualization platform https://www.bioinformatics.com.cn. The fitting process employed a cubic fitting method.

Correlation analysis

Pearson correlation analyses will be performed utilizing SPSS software in this research. The correlation plots were produced using a web-based data analysis and visualization platform https://www.bioinformatics.com.cn.

Changes in gene expression with age

Mixed-effect linear regression (MELR) model [41], utilizing the R package lme4, was employed to detect differential gene expression patterns in monocytes as they aged. This modeling strategy entails conducting linear regression analyses with both fixed-effect and random-effect terms. The fixed-effect terms evaluate the impact of age on gene expression levels, whereas the random-effect terms account for variability between different experimental batches. Specifically, cells were grouped according to their dataset source to isolate age-related gene expression changes within each dataset. In our model, the age of each donor serves as the numeric independent variable, while the log2-normalized UMI counts for each gene in each cell are utilized as the dependent variable, as demonstrated in the equation.

UMI_Expression ~ Age + Gender+ (1|Group).

In this model, age is treated as a fixed-effect factor, while gender is incorporated as a covariate to adjust for gender-related variances. The term (1|group) denotes a random-effect factor, with individual cells within each dataset designated as a group to mitigate batch-related random effects. Genes exhibiting fixed-effect amplitudes equal to or exceeding 0.002 and a false discovery rate (FDR) below 1% were deemed to be statistically significant in terms of fixed-effect amplitude alterations.

To validate our approach, we tried to remove the batch effect of gene expression using canonical correlation analysis (CCA) before MELR. Reassuringly, nearly 90% of reported age-associated genes appeared in both methods, confirming the reliability of our MELR-based correction.

Gene expression pattern analysis

Linear regression analysis was employed to identify the significant upregulation or downregulation of genes with distinct age-related gene expression patterns within individual clusters. The AverageExpression function in Seurat was utilized to determine the average gene expression level, while the raw UMI count matrix was employed to identify cells expressing the genes of interest. The Pearson correlation analysis method was utilized to evaluate the relationship between gene expression features and age, with a significance level of $p < 0.05$ set as the threshold for identifying age-related alterations. Genes exhibiting significant changes in expression patterns based on Pearson correlation analysis at $p < 0.05$ were categorized as showing percentage changes, expression changes, or a combination of both. Genes that did not demonstrate alterations in at least 5% of measurements were excluded from further analysis.

Cell age estimation

This study utilized a linear regression approach to develop a predictive model for estimating cell age by incorporating a machine learning technique centered on a random forest model or a Bayesian model. The log2-normalized gene expression values were utilized as predictive variables for determining cell age. Tenfold cross-validation was performed, with 90% of the cells randomly selected for training and the remaining 10% for testing in each fold. Each iteration of the tenfold cross-validation procedure was replicated ten times, resulting in a total of 100 repetitions. Models were evaluated based on performance (mean absolute error (MAE) and consistency. Supplementary Table 3 lists the age and gender of all participants utilized to develop the model.

Results

Older individuals and offspring of mothers with gestational diabetes had increased activity in established aging-related genes in their monocytes

The single-cell sequencing data of immune cells from all participants were analyzed, leading to the identification of $CD4^+$ T cells, $CD8^+$ T cells, B cells, NK cells, monocytes, granulocytes, and DCs based on established markers (Fig. 1a-b). Curves were generated to illustrate the variations in cell proportions with age for each cell type (Fig. 1c). Data from 56 healthy individuals aged 0-100 years were used to demonstrate the characteristics of immunosenescence. Notably, monocyte proportions fluctuated throughout the lifespan, reaching a peak in cord blood and subsequently declining in children and elderly individuals. In contrast to other cell types, the trajectory of monocyte quantity with age appeared to be inconsistent across different life stages. The upregulation of the established aging-related genes CDKN1A and CDKN2A [42] was correlated with advancing age in immune cells (Figure S1 a-f), which was particularly evident in monocytes (Fig. 1d). Moreover, the increased expression of CDKN1A and CDKN2A in the GDM group was predominantly localized in monocytes (Fig. 1e). Thus, it is postulated that monocyte aging represents the primary phenotype of immune aging induced by GDM. However, upon further stratification of the sample by age, the previously observed linear relationships between CDKN1A and CDKN2A expression and age exhibited a decreasing trend (Fig. 1f). Moreover, the analysis of cell cycle progression in monocytes of varying ages demonstrated a progressive decline in G2/S phase cells with increasing age, and the most obvious change in the GDM group was predominantly localized in monocytes (Fig. 1g). However, the correlation between cell cycle progression and age was not strong (Figure S2 a-f), suggesting that traditional markers of aging may not accurately reflect the immunological age of monocytes.

Variability in transcriptional characteristics among monocyte subclusters

Seurat was utilized to partition monocytes into 8 distinct clusters based on their gene expression similarities (Fig. 2a). c6 was identified as a nonclassical monocyte, c9 was identified as an intermediate monocyte, and the remaining 7 clusters were identified as classical monocytes (Fig. 2b-c). c1 exhibited high expression levels in antigen processing and presentation pathways, while c2 and c4 showed upregulation in lipogenesis pathways. c3 demonstrated high expression levels in pathways associated with cell proliferation and differentiation. The biosynthetic pathway of c5 was upregulated, while c7 exhibited high expression of the IFN-γ response pathway (Fig. 2d). c8 is characterized by elevated expression of the inflammatory cytokine genes IL1B and CXCL8 (Fig. 2b), heightened activation of inflammation- and apoptosis-related pathways (Fig. 2d), and increased activity of the IL18 signaling pathway (Fig. 2e). CytoTrace revealed that c3 exhibited the least degree of differentiation, whereas c8, characterized by elevated levels of inflammatory cytokines, displayed the highest level of differentiation (Fig. 2f-g).

Alterations in monocyte composition and functionality as individuals age

We analyzed how age affects monocyte clusters by examining the relationships between age and the

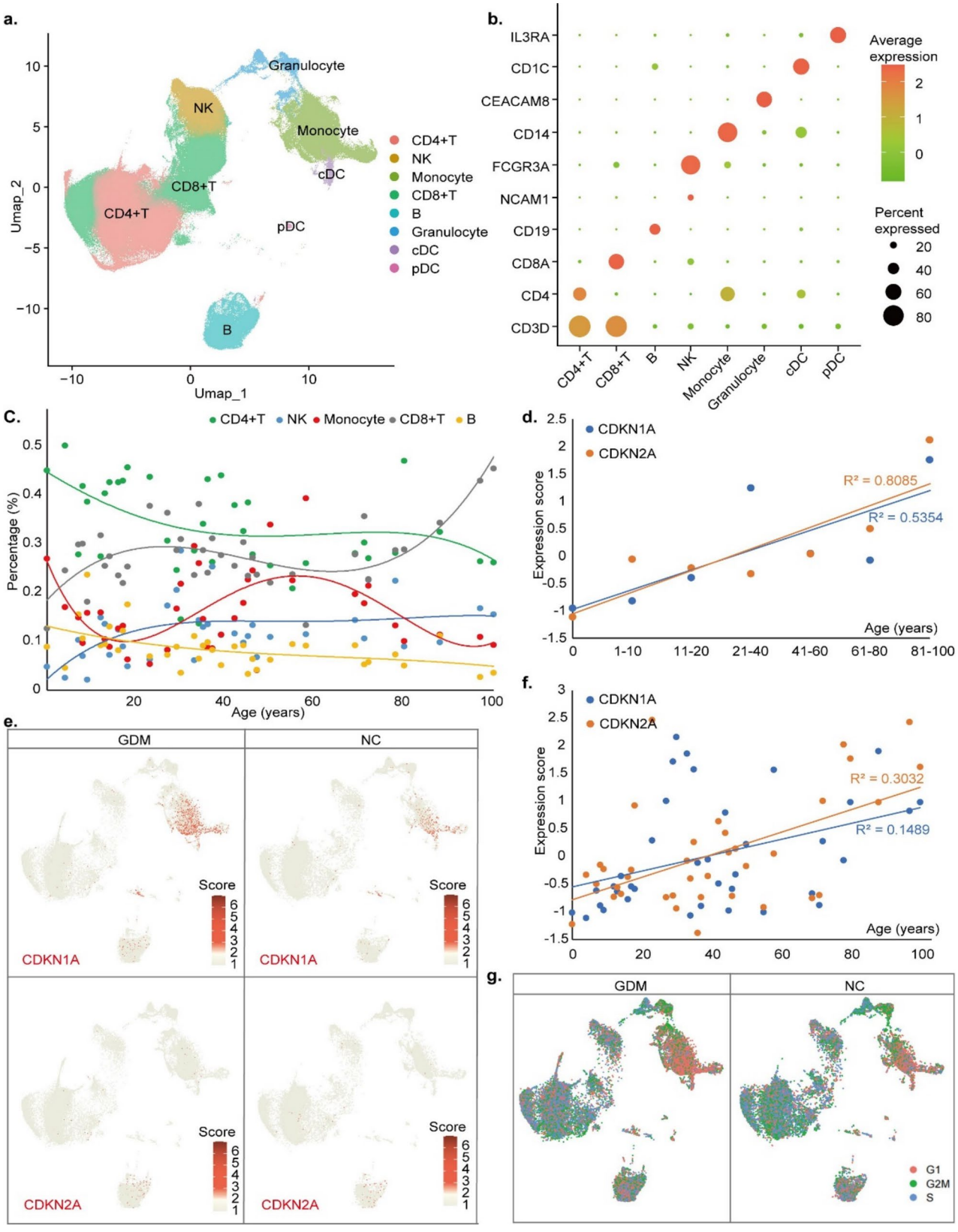

Fig. 1 (See legend on next page.)

(See figure on previous page.)

Fig. 1 The impact of age and adverse intrauterine conditions on monocytes as determined by recognized indicators of cellular senescence (**a**) UMAP visualization displaying the clusters of all immune cells (**b**) Dotplot illustrating the marker genes of each immune cell (**c**) Scatter plots were generated to depict the relationship between the proportion of immune cells in healthy individuals and age, and linear regression was used for curve fittingn (**d, f**) The scatter plots illustrate the mean expression levels of CDKN1A and CDKN2A in monocytes of individuals without health conditions across various age groups (**d**) or at different ages (**f**). Linear regression was used to model the data, and the Pearson correlation coefficient (R^2) was used to quantify the relationship between the expression of aging-related genes and chronological age (**e**) The feature plot analysis illustrates the differential expression patterns of established age-related genes in cord blood immune cells of offspring born to mothers with gestational diabetes mellitus (GDM) compared to those born to healthy controls (**g**) Cell cycle prediction results showing the distribution of cells in the G1, G2/M, and S phases

proportions of different clusters and their gene expression profiles using linear regression (Fig. 3a). Certain monocyte clusters remain stable in proportion throughout life, while others show variations with age. Less differentiated clusters c3 and c5 are more prevalent in early life and decrease with age, while clusters c4, c1, and c2 peak between ages 20 and 30 years before declining. The c8 monocyte cluster increases with age, becoming the most common in individuals over 70 years of age. Changes in the monocyte transcriptome with age were examined using the MELR analysis method. Genes with significant expression level changes were identified within specific clusters, with age as a fixed effect, sex as a covariate, and dataset source as a random effect. Genes displaying a fixed-effect amplitude of ≥ 0.002 and a false discovery rate (FDR) of < 0.01 were categorized as significantly age-related genes. These genes were identified as monocyte age-related genes. The expression of 333 genes, including FOSL1, TMP1, CXCL16, NFKB2, and MAP2K3, increased with age. The expression of 1092 genes, including PHF20, NASP, MT-ND3, CAMP, and GPSM2, decreased with age. Functional enrichment analysis revealed that these genes were mainly enriched in ferroptosis, the VEGFA-VEGFR2 and IL-18 signaling pathways, and autophagy (Fig. 3b). On the other hand, genes that were less active as individuals aged were mainly involved in the cell cycle, cell division, and protein transport pathways (Figure S3). Within each monocyte cluster, there were differences in the expression levels of these age-related genes, with most genes showing consistent trends but varying degrees of change (Fig. 3c). The upregulation of age-positively correlated genes in c8 exhibited the most notable increase with age, whereas the downregulation of age-negatively correlated genes in c3 and c5 showed the most pronounced decrease. This suggests significant alterations in the quantity and functionality of these monocyte types during aging. Our research revealed the transcriptional characteristics of these genes and potential shifts in their functional properties.

The gene expression of individual monocytes exhibits two distinct patterns of changes in relation to age

After identifying age-related gene changes, we analyzed gene expression in individual monocytes, as previously described [29]. We identified two patterns of age-related gene expression changes: changes in the percentage of positive cells and changes in gene expression levels within individual cells. We then quantified the raw UMI values of age-related genes in each cell and calculated the percentage of cells expressing each gene in every sample. We analyzed gene expression changes with age using linear fitting and Pearson correlation, selecting $p < 0.05$ for significance. Among the 333 upregulated age-related genes, 191 had increased positive cell percentage (IPCP), and 244 had increased expression levels in individual cells (IEIC). A total of 181 genes displayed both patterns, while 79 did not (Fig. 4a). To understand how age affects gene expression, we analyzed genes with different patterns of change. We found that as people age, the expression of the IPCP genes increases, and the cAMP response, inflammatory response, and glycolysis decrease (Fig. 4b). On the other hand, IEIC genes are mainly involved in cell death, glycolysis, and the response to gamma interferon (Fig. 4c). Among the downregulated age-related genes, 833 had a decreased positive cell percentage (DPCP), and 832 had decreased expression levels in individual cells (DEIC). 775 genes exhibited both patterns, while 201 did not (Fig. 4d). Functional enrichment showed that with age, the DPCP and DEIC genes were mainly enriched in protein degradation metabolism and phosphorylation-related pathways (Fig. 4e-f). It can be inferred from the data that gene expression in monocytes changes with age, exhibiting two distinct patterns that may be associated with the adaptation of monocytes to varying age-related physiological conditions and immune requirements.

Construction of the immunological age prediction model for monocytes spanning the age range of 0 to 100 years

We predicted the age of monocytes by analyzing gene expression patterns using random forest and Bayesian methods and assessed the efficacy of the model through 10-fold cross-validation. The sample information used to build the model is shown in supplementary Table 3. Our analysis showed that the random forest algorithm was better than the Bayesian method at predicting age-related gene expression patterns. The final model had a MAE of 8.49 ± 0.06 and an R^2 of 0.76 for age prediction (Fig. 5a), while the Bayesian model had an MAE of 14.64 ± 0.12 and an R^2 of 0.45. Consequently, the random forest model developed for forecasting the immunological age of monocytes, denoted as "mono_age",

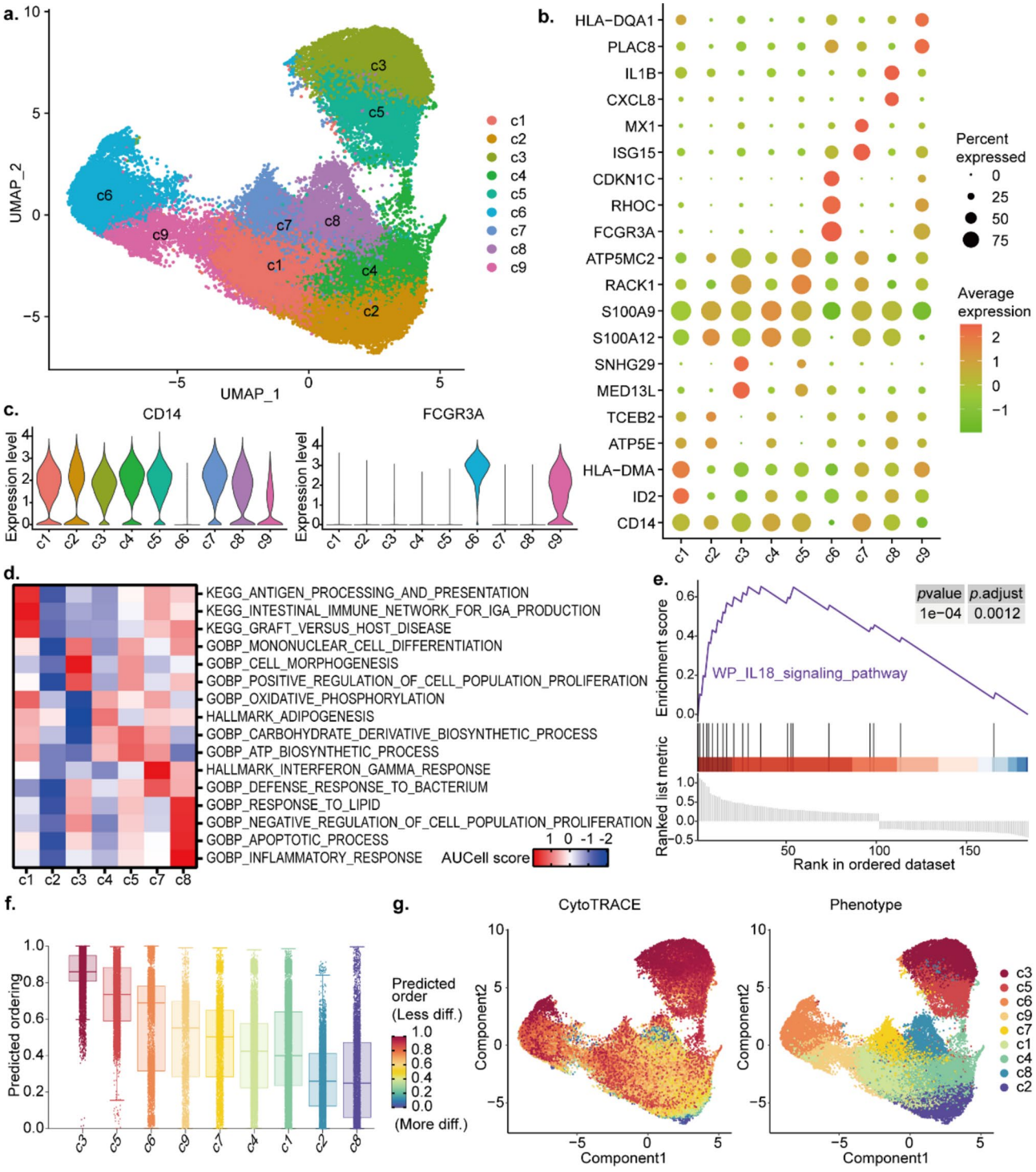

Fig. 2 Transcriptional characteristics of subclusters present within monocytes (**a**) UMAP plot showing the clusters of all monocytes (**b**) Dot plot showing the characteristic genes of each monocyte cluster (**c**) Violin diagram showing the expression of CD14 and FCGR3A (CD16) in each monocyte cluster (**d**) Heatmaps showing pathway enrichment results for each monocyte cluster. The colors represent the AUCell score (**e**) KEGG enrichment demonstrated the upregulation of the IL8 signaling pathway in c8 (**f**) The ability of CytoTrace to infer the level of cell differentiation is demonstrated through a boxplot, which illustrates the anticipated degree of differentiation within each group of monocytes (**g**) Left: CytoTrace was utilized on the left to forecast the cell cycle distribution, with colors indicating the anticipated level of differentiation. The UMAP diagram was used to visualize the anticipated cellular localization based on the differentiation level. Right: The diagram illustrates the distribution of distinct clusters within the UMAP diagram

has a distinct advantage. Notably, the predicted age of monocytes displayed variability around the actual age

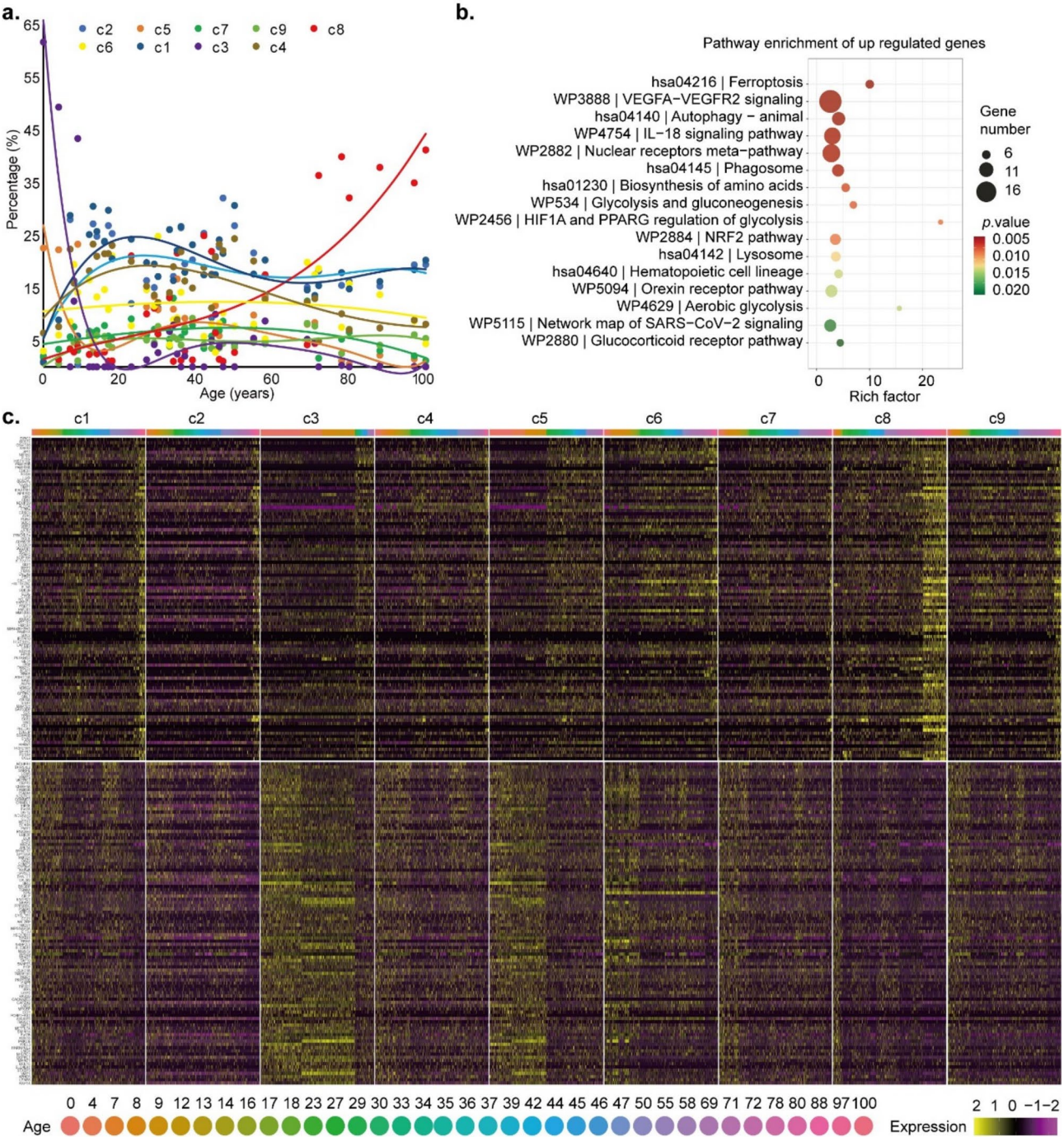

Fig. 3 Changes in monocyte composition and gene expression with age (**a**) Scatter plots showing the change in the percentage of mononuclear cells in healthy people at each age. Linear regression was used for fitting (**b**) The bubble map shows the pathway enrichment results of upregulated genes with age (**c**) Heatmaps showing age-dependent changes in the expression of upregulated (top half) and downregulated (bottom half) genes in each cluster

of the sample. A recent study highlighted immune aging in monocytes of individuals with COVID-19, revealing a correlation with disease severity [43, 44]. We used single-cell sequencing data to predict the immunological age of blood monocytes in COVID-19 patients (Fig. 5b-e). Our random forest model showed a significant difference in the predicted monocyte age between healthy controls and COVID-19 patients, with patients with severe COVID-19 having a greater predicted age than patients with mild COVID-19. Overall, our model effectively captured variations in monocyte immunological age across different levels of COVID-19 severity.

GDM leads to an elevated immunological age of umbilical cord monocytes in offspring

GDM can lead to lasting complications in offspring, including changes in their immune cells. This study aimed to further explore how GDM affects the development of monocytes in newborns. Our initial analysis focused on examining alterations in traditional aging-related genes within the GDM cohort, revealing elevated expression levels of CDKN1A and CDKN2A in cord blood monocytes from individuals with GDM compared to those from healthy controls (Fig. 6a-b). Subsequent cell cycle analysis indicated a greater proportion of cells in the G1 phase in the GDM group than in the control group, suggesting a diminished proliferative capacity (Fig. 6c-d). Additionally, alterations in age-related genes within the GDM group were assessed. Out of the 216 age-upregulated genes present in cord blood, 169 genes exhibited upregulation in the GDM group (Fig. 6e). Conversely, among the 1091 age-downregulated genes in cord blood, 483 genes were downregulated in the GDM group (Fig. 6f). This finding indicates a potential substantial influence of GDM on age-upregulated genes, leading to a subsequent investigation into the distribution of genes exhibiting varying degrees of upregulation. Among the 169 age-upregulated genes upregulated in the GDM group, 81 genes exhibited over 25% increased expression relative to controls, with 43 genes exhibited over 50% increased (Fig. 6g). PPI analysis of these 43 genes revealed enrichment of genes involved in the glucocorticoid receptor pathway, the IL-18 signaling pathway, and the regulation of apoptotic processes (Fig. 6h). Subsequently, we used the random forest model to predict the mono_age of cord blood monocytes from GDM donors compared to healthy controls (Fig. 6i). Despite a smaller sample size, we found that the average mono_age of cord blood monocytes from the GDM group was greater than that of the healthy control group, equivalent to an increase of approximately 2 years in actual age ($p = 0.057$). We found that the immune age of cord blood monocytes was negatively correlated with maternal weight gain during pregnancy and free fatty acid content in cord blood (Fig. 6j, Figure S4 a) but was positively correlated with the highest fasting blood glucose levels during pregnancy and cord blood C-peptide levels (Fig. 6k, Figure S4 b). This suggests that GDM may impact the immune age of offspring monocytes through abnormal glucose and lipid metabolism.

Discussion

Our research presents the initial single-cell immune atlas of monocytes spanning the age range from 0 to 100 years, elucidating the cluster distribution and gene expression profiles of monocytes throughout the lifespan. Additionally, we developed the first model for estimating the age of monocytes and observed aging-related traits and elevated immune age predictions in cord blood monocytes following GDM exposure, indicating a potential link between GDM exposure in utero and premature aging of offspring monocytes.

Our past research showed that offspring monocytes from GDM pregnancies produce more inflammatory factors, such as IL1B and CXCL8 [16]. This suggests that GDM may affect the aging of monocytes. Previous studies have also shown accelerated aging of muscle cells, endothelial cells, and mesenchymal stem cells in the offspring of GDM pregnancies [9–11], as well as shorter telomeres in leukocytes [12]. This study suggested that exposure to abnormal glucose tolerance in the intrauterine environment during fetal development may expedite age-related transcriptional alterations in monocytes, resulting in the premature emergence of a proinflammatory phenotype. Consequently, timely intervention to prevent age-related diseases in offspring monocytes exposed to GDM is imperative.

Previous research has shown an increase in intermediate and nonclassical monocytes in older populations [45]. Our study confirmed this trend in the 70- to 80-year-old group compared to the 30- to 60-year-old group. However, we also observed elevated levels in the 10–30 age group, which decreased after 70 years, possibly due to our study's wider age range and detailed breakdown. A specific subset of classical monocytes with high IL1B and CXCL8 levels increased with age, particularly in individuals over 70 years of age. In summary, our study revealed a new type of aging in monocytes, with increased numbers of $IL1B^+CXCL8^+$ classical monocytes in people older than 70 years. This subset showed increased inflammation-related pathways, similar to the SASP.

MELR analysis revealed age-related gene expression changes in monocytes, with two patterns observed as age increased: changes in expression levels within cells or in the number of cells expressing the gene. These finding parallels previous findings in $CD8^+$ T cells [29], which we simplified into two patterns for clarity. Due to the variation in gene expression patterns with age, we used a random forest method to predict monocyte immune age in healthy individuals. Previous studies have shown that monocytes in severely ill COVID-19 patients age faster than those in mildly ill patients and healthy individuals [43, 44]. Our results support this finding, highlighting the accuracy of the random forest model in predicting immune age.

Our study is subject to several limitations. First, the samples collected from various age groups were obtained from distinct individuals, potentially leading to variations in immune cell status due to genetic and environmental influences. Consequently, longitudinal sampling of the same participants in the future is essential to corroborate

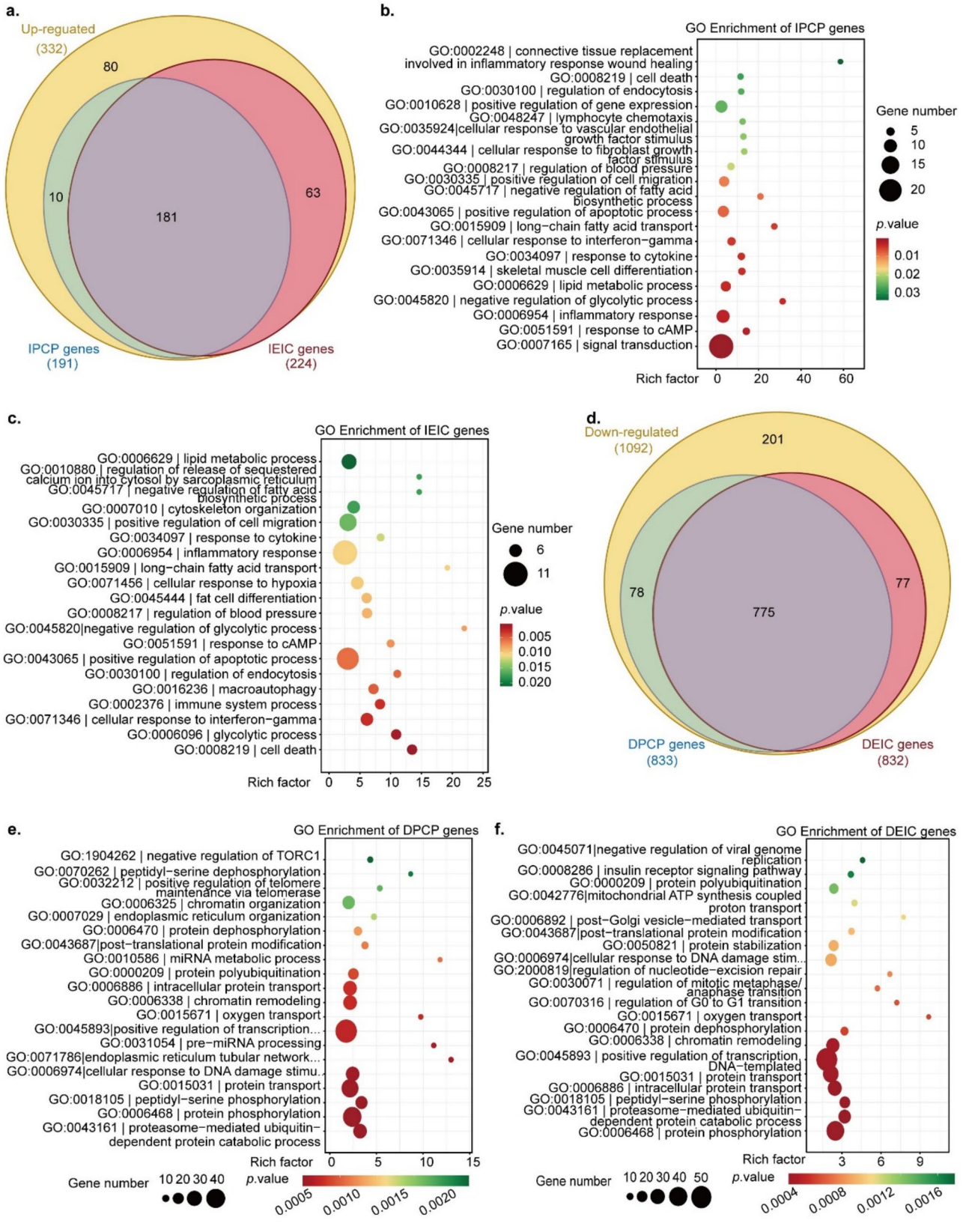

Fig. 4 (See legend on next page.)

(See figure on previous page.)

Fig. 4 Two patterns of age-related genes (**a**) Venn diagram showing the distribution and quantity of two patterns of change in genes upregulated with age. IPCP: Increased positive cell percentage; IEIC: Increased expression levels in individual cells (**b**) Bubble maps showing the results of GOBP functional enrichment of genes with an increased number of positive cells (**c**) Bubble maps showing the results of GOBP functional enrichment of genes with increased expression in individual cells (**d**) Venn diagram showing the distribution and quantity of two patterns of change in genes downregulated with age. DPCP: Decreased positive cell percentage; DEIC: Decreased expression levels in individual cells (**e**) Bubble maps showing the results of GOBP functional enrichment for genes with reduced positive cell numbers (**f**) Bubble map showing the results of GOBP functional enrichment of genes with reduced expression in a single cell

our results. Second, despite efforts to mitigate batch effects through removal and normalization analyses of publicly available datasets, the presence of batch discrepancies cannot be entirely discounted. Finally, while the age of our GDM patient cohort was adequately matched with that of the healthy control group, the restricted sample size underscores the need for additional large-scale investigations to corroborate our findings.

Conclusions

This study revealed changes in monocyte gene expression with age, created a model to predict monocyte immune age, and showed that exposure to adverse conditions in utero due to GDM accelerates aging in offspring monocytes. Maternal weight gain, high fasting blood glucose levels, and cord blood C-peptide levels during pregnancy are key factors in this effect. Research shows that managing weight and blood glucose levels in pregnant women with GDM is important for reducing the impact on their children's immune system.

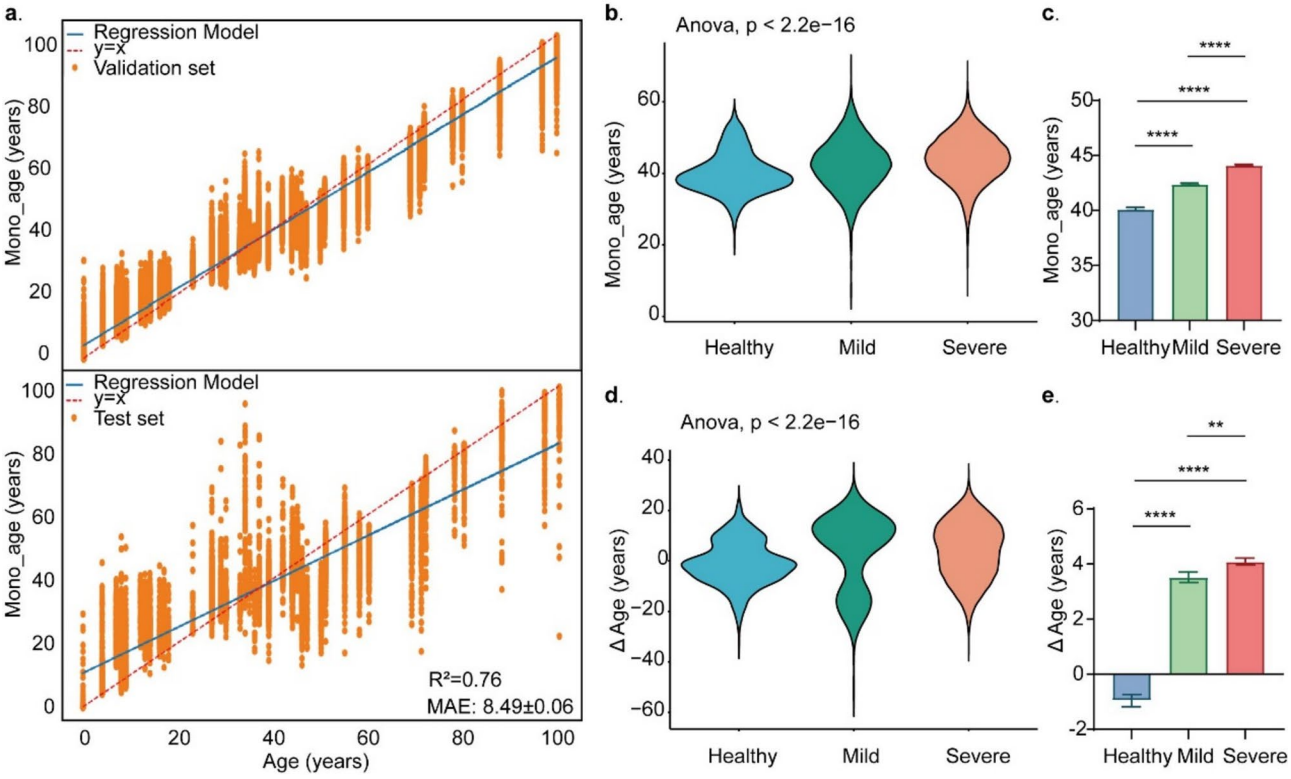

Fig. 5 Construction of the immune age prediction model (**a**) The prediction results of the random forest prediction model in the training set (top) and the test set (bottom). The Pearson correlation coefficient (R^2) was utilized to quantify the relationship between the predicted age and the actual age (**b**) Violin chart showing the age prediction of monocytes in healthy controls and patients with mild or severe COVID-19 in the GSE206283 dataset at first admission. One-way ANOVA was used to calculate the difference between the groups (**c**) Bar chart showing the age prediction of monocytes in healthy controls and patients with mild or severe COVID-19 at first admission. An independent t test was used to calculate the differences between the groups (**d**) Violin plot showing the difference between the predicted age of monocytes and the actual age at first admission to the hospital in healthy controls and patients with mild or severe COVID-19. One-way ANOVA was used to calculate differences between groups (**e**) The bar chart shows the difference between the predicted age of monocytes and the actual age of healthy controls and mild or patients with severe COVID-19 when they were first admitted. The difference between groups was calculated using independent t tests

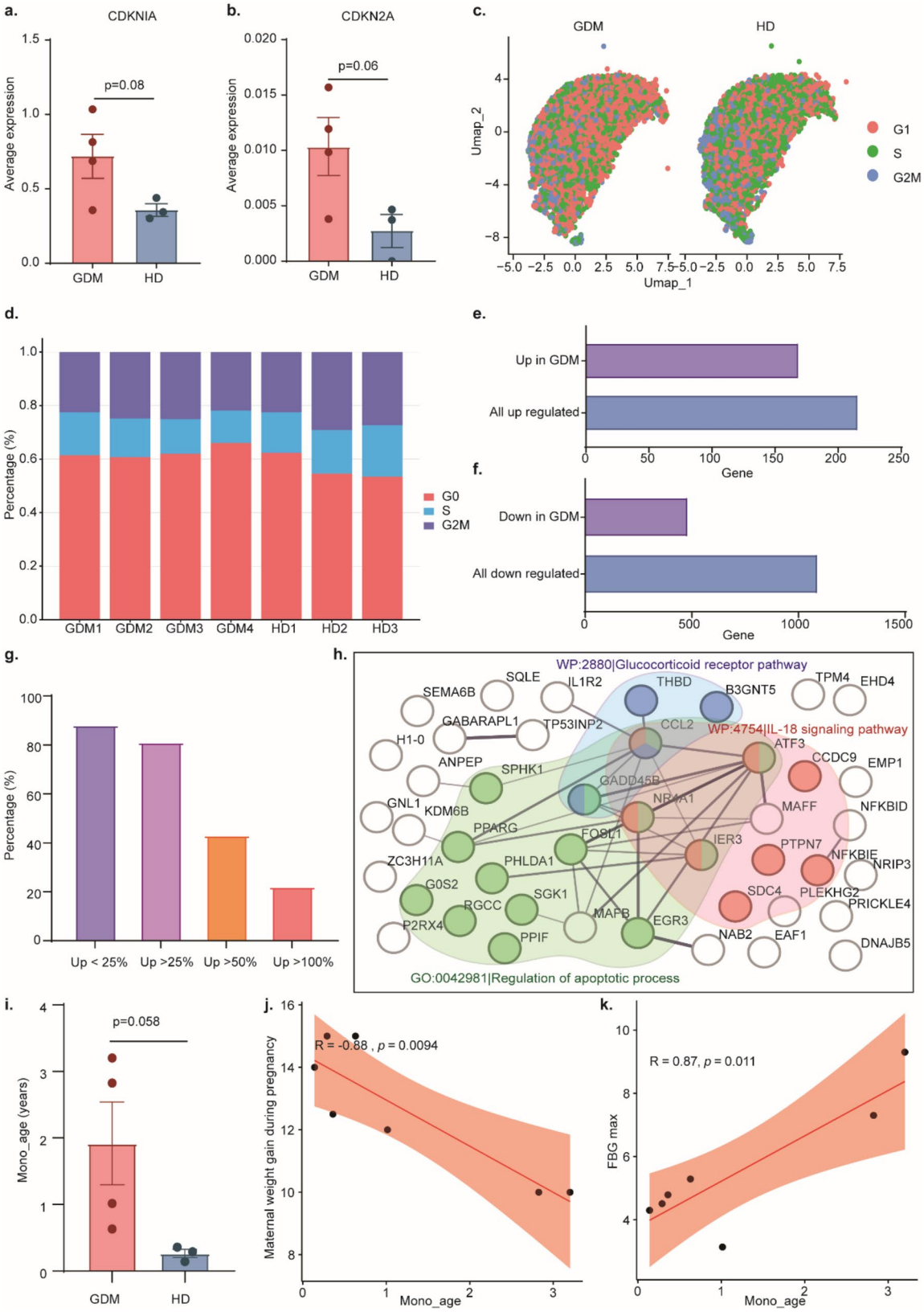

Fig. 6 (See legend on next page.)

(See figure on previous page.)

Fig. 6 Gestational diabetes mellitus can lead to increased age of mononuclear immunity in umbilical blood (**a-b**) Expression of the classical age-related genes CDKN1A (**a**) and CDKN2A (**b**) in GDM progeny and healthy control homoharmonic mononuclear cells (**c**) Distribution of different cell cycle phases of monocytes in the umbilical blood of the two groups (**d**) The distribution of different cell cycle phases in each cord blood sample (**e**) Bar plots showing the number of genes upregulated with age detected in cord blood and the number of genes increased in the GDM group (**f**) Bar plots showing the number of genes downregulated with age detected in cord blood and the number of genes downregulated in the GDM group (**g**) Distribution of genes with different fold increases in the GDM group (**h**) Upregulated protein–protein interactions between more than 50% of genes in the GDM group (**i**) Two groups of umbilical blood mononuclear cells were analyzed using a random forest model to predict immune age (**j-k**) Correlations between cord blood mononuclear cell levels, which predict age and pregnancy weight gain (**j**), and maximum fasting blood glucose levels (**k**). The *p* value was calculated using Pearson correlation

Supplementary Information

The online version contains supplementary material available at https://doi.org/10.1186/s12979-025-00513-z.

Supplementary Material 1

Supplementary Material 2

Supplementary Material 3

Acknowledgements

We thank Dr. Jacques for providing the GEO dataset GSE135779, Dr. Ren for providing the GEO dataset GSE158055, Dr. Giroux for providing the GEO dataset GSE206283, and Dr. Luo for providing the GEO dataset GSE157007. We thank Pro. Wen Deng for providing clinical information and sample collection of umbilical cord blood. We thank Yu Zhang for helping with sample collection and isolation.

Author contributions

X.L. conceived and supervised the project. Y.Z.,T.Z. and M.Y. recruited the subjects. Y.Z. and R.G. performed the bioinformatic analysis. Y.Z. wrote the manuscript. S.S.L., M.S., and X.L. revised the manuscript. All authors discussed and approved the manuscript submission.

Funding

This study was supported by the National Key R&D Program of China(2022YFC2010102), the National Natural Science Foundation of China (grant no. 82070812), the Natural Science Foundation of Hunan Province (2023JJ30762), the Natural Science Foundation of Hunan Province (grant no. 2024JJ6581), China Postdoctoral Science Foundation (grant 2024M753697), the Postdoctoral Fellowship Program of CPSF (grant no. GZC20233190), and the Natural Science Foundation of Hunan Province (2025JJ60688).

Data availability

The raw scRNA-seq datasets in the FASTQ format with filtered barcode matrix have been uploaded to the Gene Expression Omnibus (GEO) database: GSE212309 and GSE221297. The publicly available PBMC scRNA-sequencing data used in the study are available in GEO with the accession number GSE158055, GSE135779, GSE157007, and GSE206283. The information for single-cell sequencing is available in Supplementary Tables.

Declarations

Competing interests

The authors declare no competing interests.

Received: 16 July 2024 / Accepted: 26 April 2025
Published online: 13 May 2025

References

1. Saravanan P. Gestational diabetes: opportunities for improving maternal and child health. Lancet Diabets Endocrionol. 2020;8:793–800. https://doi.org/10.1016/s2213-8587(20)30161-3.
2. McIntyre HD, Catalano P, Zhang C, Desoye G, Mathiesen ER, Damm P. Gestational diabetes mellitus. Nat Reviews Disease Primers. 2019;5. https://doi.org/10.1038/s41572-019-0098-8.
3. Zhang C, Catalano P. Screening for gestational diabetes. JAMA. 2021;326:487–9. https://doi.org/10.1001/jama.2021.12190.
4. Sweeting A, Wong J, Murphy HR, Ross GP. A clinical update on gestational diabetes mellitus. Endocr Rev. 2022. https://doi.org/10.1210/endrev/bnac003.
5. Ye W, Luo C, Huang J, Li C, Liu Z, Liu F. Gestational diabetes mellitus and adverse pregnancy outcomes: systematic review and meta-analysis. BMJ. 2022;377:e067946. https://doi.org/10.1136/bmj-2021-067946.
6. Lowe WL Jr., Scholtens DM, Kuang A, Linder B, Lawrence JM, Lebenthal Y, McCance D, Hamilton J, Nodzenski M, Talbot O, et al. Hyperglycemia and adverse pregnancy outcome Follow-up study (HAPO FUS): maternal gestational diabetes mellitus and childhood glucose metabolism. Diabetes Care. 2019;42:372–80. https://doi.org/10.2337/dc18-1646.
7. Grunnet LG, Hansen S, Hjort L, Madsen CM, Kampmann FB, Thuesen ACB, Granstrømi C, Strøm M, Maslova E, Frikke-Schmidt R, et al. Adiposity, dysmetabolic traits, and earlier onset of female puberty in adolescent offspring of women with gestational diabetes mellitus: A clinical study within the Danish National birth cohort. Diabetes Care. 2017;40:1746–55. https://doi.org/10.2337/dc17-0514.
8. Gui J, Rohrbach A, Borns K, Hillemanns P, Feng L, von Hubel CA. Versen-Höynck, F. Vitamin D rescues dysfunction of fetal endothelial colony forming cells from individuals with gestational diabetes. Placenta. 2015;36:410–8. https://doi.org/10.1016/j.placenta.2015.01.195.
9. Blue EK, DiGiuseppe R, Derr-Yellin E, Acosta JC, Pay SL, Hanenberg H, Schellinger MM, Quinney SK, Mund JA, Case J, et al. Gestational diabetes induces alterations in the function of neonatal endothelial colony-forming cells. Pediatr Res. 2014;75:266–72. https://doi.org/10.1038/pr.2013.224.
10. Kong CM, Subramanian A, Biswas A, Stunkel W, Chong YS, Bongso A, Fong CY. Changes in stemness properties, differentiation potential, oxidative stress, senescence and mitochondrial function in Wharton's jelly stem cells of umbilical cords of mothers with gestational diabetes mellitus. Stem Cell Rev Rep. 2019;15:415–26. https://doi.org/10.1007/s12015-019-9872-y.
11. Palma C, McIntyre HD, Salomon C. Extracellular Vesicles-New players in Cell-to-Cell communication in gestational diabetes mellitus. Biomedicines. 2022;10. https://doi.org/10.3390/biomedicines10020462.
12. Xu J, Ye J, Wu Y, Zhang H, Luo Q, Han C, Ye X, Wang H, He J, Huang H, et al. Reduced fetal telomere length in gestational diabetes. PLoS ONE. 2014;9:e86161. https://doi.org/10.1371/journal.pone.0086161.
13. Teo YV, Rattanavirotkul N, Olova N, Salzano A, Quintanilla A, Tarrats N, Kiourtis C, Müller M, Green AR, Adams PD, et al. Notch signaling mediates secondary senescence. Cell Rep. 2019;27:997–e10071005. https://doi.org/10.1016/j.celrep.2019.03.104.
14. Isermann A, Mann C, Rübe CE, Histone Variant. H2A.J marks persistent DNA damage and triggers the secretory phenotype in Radiation-Induced senescence. Int J Mol Sci. 2020;21. https://doi.org/10.3390/ijms21239130.
15. Liu Z, Liang Q, Ren Y, Guo C, Ge X, Wang L, Cheng Q, Luo P, Zhang Y, Han X. Immunosenescence: molecular mechanisms and diseases. Signal Transduct Target Ther. 2023;8:200. https://doi.org/10.1038/s41392-023-01451-2.
16. Yin M, Zhang Y, Li X, Liu S, Huang J, Yu H, Li X. Adverse effects of gestational diabetes mellitus on fetal monocytes revealed by single-cell RNA sequencing. iScience. 2024;27:108637. https://doi.org/10.1016/j.isci.2023.108637.
17. Cao Y, Fan Y, Li F, Hao Y, Kong Y, Chen C, Hao X, Han D, Li G, Wang Z, et al. Phenotypic and functional alterations of monocyte subsets with aging. Immun Ageing. 2022;19:63. https://doi.org/10.1186/s12979-022-00321-9.
18. Cheong CY, Yap P, Yap KB, Ng TP. Associations of inflammatory, metabolic, malnutrition, and frailty indexes with Multimorbidity incidence and progression, and mortality impact: Singapore longitudinal aging study. Gerontology. 2023;69:416–27. https://doi.org/10.1159/000527428.
19. Puchta A, Naidoo A, Verschoor CP, Loukov D, Thevaranjan N, Mandur TS, Nguyen PS, Jordana M, Loeb M, Xing Z, et al. TNF drives monocyte

dysfunction with age and results in impaired Anti-pneumococcal immunity. PLoS Pathog. 2016;12:e1005368. https://doi.org/10.1371/journal.ppat.1005368.
20. Hearps AC, Martin GE, Angelovich TA, Cheng WJ, Maisa A, Landay AL, Jaworowski A, Crowe SM. Aging is associated with chronic innate immune activation and dysregulation of monocyte phenotype and function. Aging Cell. 2012;11:867–75. https://doi.org/10.1111/j.1474-9726.2012.00851.x.
21. Vellasamy DM, Lee SJ, Goh KW, Goh BH, Tang YQ, Ming LC, Yap WH. Targeting immune senescence in atherosclerosis. Int J Mol Sci. 2022;23. https://doi.org/10.3390/ijms232113059.
22. Terekhova M, Swain A, Bohacova P, Aladyeva E, Arthur L, Laha A, Mogilenko DA, Burdess S, Sukhov V, Kleverov D, et al. Single-cell atlas of healthy human blood unveils age-related loss of NKG2C(+)GZMB(-)CD8(+) memory T cells and accumulation of type 2 memory T cells. Immunity. 2024;57:188–92. https://doi.org/10.1016/j.immuni.2023.12.014.
23. Zhang C, Zhang X, Huang L, Guan Y, Huang X, Tian XL, Zhang L, Tao W. ATF3 drives senescence by reconstructing accessible chromatin profiles. Aging Cell. 2021;20:e13315. https://doi.org/10.1111/acel.13315.
24. Cruickshanks HA, McBryan T, Nelson DM, Vanderkraats ND, Shah PP, van Tuyn J, Singh Rai T, Brock C, Donahue G, Dunican DS, et al. Senescent cells harbour features of the cancer epigenome. Nat Cell Biol. 2013;15:1495–506. https://doi.org/10.1038/ncb2879.
25. Shireby GL, Davies JP, Francis PT, Burrage J, Walker EM, Neilson GWA, Dahir A, Thomas AJ, Love S, Smith RG, et al. Recalibrating the epigenetic clock: implications for assessing biological age in the human cortex. Brain. 2020;143:3763–75. https://doi.org/10.1093/brain/awaa334.
26. Peters MJ, Joehanes R, Pilling LC, Schurmann C, Conneely KN, Powell J, Reinmaa E, Sutphin GL, Zhernakova A, Schramm K, et al. The transcriptional landscape of age in human peripheral blood. Nat Commun. 2015;6:8570. https://doi.org/10.1038/ncomms9570.
27. Fleischer JG, Schulte R, Tsai HH, Tyagi S, Ibarra A, Shokhirev MN, Huang L, Hetzer MW, Navlakha S. Predicting age from the transcriptome of human dermal fibroblasts. Genome Biol. 2018;19:221. https://doi.org/10.1186/s13059-018-1599-6.
28. Alpert A, Pickman Y, Leipold M, Rosenberg-Hasson Y, Ji X, Gaujoux R, Rabani H, Starosvetsky E, Kveler K, Schaffert S, et al. A clinically meaningful metric of immune age derived from high-dimensional longitudinal monitoring. Nat Med. 2019;25:487–95. https://doi.org/10.1038/s41591-019-0381-y.
29. Lu J, Ahmad R, Nguyen T, Cifello J, Hemani H, Li J, Chen J, Li S, Wang J, Achour A, et al. Heterogeneity and transcriptome changes of human CD8(+) T cells across nine decades of life. Nat Commun. 2022;13:5128. https://doi.org/10.1038/s41467-022-32869-x.
30. Zhong T, Li X, Lei K, Tang R, Deng Q, Love PE, Zhou Z, Zhao B, Li X. TGF-β-mediated crosstalk between TIGIT(+) Tregs and CD226(+)CD8(+) T cells in the progression and remission of type 1 diabetes. Nat Commun. 2024;15:8894. https://doi.org/10.1038/s41467-024-53264-8.
31. Ren X, Wen W, Fan X, Hou W, Su B, Cai P, Li J, Liu Y, Tang F, Zhang F, et al. COVID-19 immune features revealed by a large-scale single-cell transcriptome atlas. Cell. 2021;184:1895–e19131819. https://doi.org/10.1016/j.cell.2021.01.053.
32. Luo OJ, Lei W, Zhu G, Ren Z, Xu Y, Xiao C, Zhang H, Cai J, Luo Z, Gao L. Multidimensional single-cell analysis of human peripheral blood reveals characteristic features of the immune system landscape in aging and frailty. Nat Aging. 2022;2:348–64.
33. Nehar-Belaid D, Hong S, Marches R, Chen G, Bolisetty M, Baisch J, Walters L, Punaro M, Rossi RJ, Chung CH, et al. Mapping systemic lupus erythematosus heterogeneity at the single-cell level. Nat Immunol. 2020;21:1094–106. https://doi.org/10.1038/s41590-020-0743-0.
34. Giroux NS, Ding S, McClain MT, Burke TW, Petzold E, Chung HA, Rivera GO, Wang E, Xi R, Bose S, et al. Differential chromatin accessibility in peripheral blood mononuclear cells underlies COVID-19 disease severity prior to seroconversion. Sci Rep. 2022;12. https://doi.org/10.1038/s41598-022-15668-8.
35. Becht E, McInnes L, Healy J, Dutertre CA, Kwok IWH, Ng LG, Ginhoux F, Newell EW. Dimensionality reduction for visualizing single-cell data using UMAP. Nat Biotechnol. 2018. https://doi.org/10.1038/nbt.4314.
36. Guilliams M, Bonnardel J, Haest B, Vanderborght B, Wagner C, Remmerie A, Bujko A, Martens L, Thoné T, Browaeys R, et al. Spatial proteogenomics reveals distinct and evolutionarily conserved hepatic macrophage niches. Cell. 2022;185:379–e396338. https://doi.org/10.1016/j.cell.2021.12.018.
37. Aibar S, González-Blas CB, Moerman T, Huynh-Thu VA, Imrichova H, Hulselmans G, Rambow F, Marine JC, Geurts P, Aerts J, et al. SCENIC: single-cell regulatory network inference and clustering. Nat Methods. 2017;14:1083–6. https://doi.org/10.1038/nmeth.4463.
38. GSEA. database.http://www.gsea-msigdb.org/gsea.last accessed on 30 July 2022.
39. ggplot2 R package. https://cran.r-project.org/web/packages/ggplot2/index.html.last accessed on 30 July 2022.
40. Gulati GS, Sikandar SS, Wesche DJ, Manjunath A, Bharadwaj A, Berger MJ, Ilagan F, Kuo AH, Hsieh RW, Cai S, et al. Single-cell transcriptional diversity is a hallmark of developmental potential. Science. 2020;367:405–11. https://doi.org/10.1126/science.aax0249.
41. Bates D, Mächler M, Bolker B, Walker S. Fitting linear Mixed-Effects models using lme4. J Stat Softw. 2015;67:1–48. https://doi.org/10.18637/jss.v067.i01.
42. Windener F, Grewing L, Thomas C, Dorion MF, Otteken M, Kular L, Jagodic M, Antel J, Albrecht S, Kuhlmann T. Physiological aging and inflammation-induced cellular senescence May contribute to oligodendroglial dysfunction in MS. Acta Neuropathol. 2024;147:82. https://doi.org/10.1007/s00401-024-02733-x.
43. Pence BD. Aging and monocyte immunometabolism in COVID-19. Aging. 2021;13:9154–5. https://doi.org/10.18632/aging.202918.
44. Lin Y, Postma DF, Steeneken LS, Melo Dos Santos LS, Kirkland JL, Espindola-Netto JM, Tchkonia T, Borghesan M, Bouma HR, Demaria M. Circulating monocytes expressing senescence-associated features are enriched in COVID-19 patients with severe disease. Aging Cell. 2023;22:e14011. https://doi.org/10.1111/acel.14011.
45. Ong SM, Hadadi E, Dang TM, Yeap WH, Tan CT, Ng TP, Larbi A, Wong SC. The pro-inflammatory phenotype of the human non-classical monocyte subset is attributed to senescence. Cell Death Dis. 2018;9:266. https://doi.org/10.1038/s41419-018-0327-1.

Publisher's note